Research Article | Vol. 29, No. 6 / 15 March 2021 / Optics Express 8985
Optics EXPRESS

Spectrally resolved point-spread-function engineering using a complex medium

ANTOINE BONIFACE,[1,*] MICKAEL MOUNAIX,[1,2] BAPTISTE BLOCHET,[1,3] HILTON B. DE AGUIAR,[1] FABIEN QUÉRÉ,[4] AND SYLVAIN GIGAN[1]

[1]Laboratoire Kastler Brossel, ENS-Université PSL, CNRS, Sorbonne Université, Collège de France, 24 rue Lhomond, 75005 Paris, France
[2]School of Information Technology and Electrical Engineering, The University of Queensland, Brisbane, QLD, 4072, Australia
[3]Department of Electrical Engineering, California Institute of Technology, Pasadena, CA 91125, USA
[4]Université Paris-Saclay, CEA, CNRS, LIDYL, 91191, Gif-sur-Yvette, France
*antoine.boniface@lkb.ens.fr

Abstract: Propagation of an ultrashort pulse of light through strongly scattering media generates an intricate spatio-spectral speckle that can be described by means of the multi-spectral transmission matrix (MSTM). In conjunction with a spatial light modulator, the MSTM enables the manipulation of the pulse leaving the medium; in particular focusing it at any desired spatial position and/or time. Here, we demonstrate how to engineer the point-spread-function of the focused beam both spatially and spectrally, from the measured MSTM. It consists of numerically filtering the spatial content at each wavelength of the matrix prior to focusing. We experimentally report on the versatility of the technique through several examples, in particular as an alternative to simultaneous spatial and temporal focusing, with potential applications in multiphoton microscopy.

1. Introduction

Temporal control of ultrashort pulses is a cornerstone of ultrafast optics. Pulse shaping refers to technologies that enable programmable reshaping of ultrafast optical waveforms, with control of phase, amplitude, and polarization [1]. It is now widely used in laser control over molecular and material responses [2], but also for wavelength selective switches [3] or in multiphoton microscopy to adjust the image contrast or resolution [4,5]. In general, the method relies on spatially dispersing a pulse with a diffraction grating in order to manipulate separately its frequency components.

Recent advances in very different research fields have shown that the ability to manipulate the full spatio-spectral or spatio-temporal structure of laser pulses, i.e. to introduce spatio-spectral couplings, can open new possibilities to control light propagation [6] and light-matter interaction [7–10]. Another important example of the usefulness of spatio-temporal couplings is given by simultaneous space-time focusing [11,12], now widely used in multiphoton excitation for neuroscience [5]. Although some extensions of temporal shapers to spatio-temporal control have been demonstrated [13–15] [16,17], such schemes are optically very complex, and their use has thus not become widespread. A general-purpose versatile method for spatio-spectral pulse control is still elusive.

Scattering of broadband light in disordered materials randomly mixes the spatial and spectral modes of the incident pulse. When a coherent ultrashort pulse travels through a multiply scattering medium its optical wavefront is spatially distorted and forms a speckle pattern [18]. When the bandwidth of the laser $\Delta\lambda^{\text{laser}}$ is broader than the spectral correlation bandwidth of the medium $\delta\lambda_m$, the speckle depends on the wavelength λ. Therefore, the scattering medium

#403578 https://doi.org/10.1364/OE.403578
Journal © 2021 Received 23 Jul 2020; revised 26 Feb 2021; accepted 1 Mar 2021; published 9 Mar 2021

Optics EXPRESS

acts as a dispersive optical element for ultrashort pulses of light. In this regime, the optical transformation of the field induced by the medium is very complex but still remains linear and deterministic, hence controllable. Owing to the availability of spatial light modulators (SLMs), several techniques based on wavefront shaping were developed to experimentally characterize this process. A recurrent application is to find the incident wavefront that counterbalances the effects of scattering and thus re-compress the pulse to its initial duration and focus it to a diffraction limited spot. For instance it can be achieved by iteratively optimizing the incident wavefront [19,20] but also by using digital phase conjugation [21], spectral pulse shaping [22], or time-gating techniques [23]. Another and more global approach to describe and manipulate the outgoing broadband light consists of measuring the multi-spectral transmission matrix (MSTM) [24]. The MSTM is a set of $N_\lambda \approx \Delta\lambda^{\text{laser}}/\delta\lambda_m$ monochromatic transmission matrices (TMs); each TM linearly relates the input field to the output field of the medium [25] for a given spectral component of the pulse. The full set of matrices provides both spatial and spectral/temporal information for controlling the transmitted pulse; in particular enhancing a single spectral component of the output pulse or focusing it at a given time can be performed [26–28]. The key point here is that these techniques manipulate both spatial and spectral degrees of freedom of the pulse by only using a single SLM. This is possible thanks to the spatio-spectral coupling resulting from the propagation through the medium. This is what we exploit here, now implemented as 3D spatio-spectral control, relying on a single SLM. Although pulse control in complex media has already been studied in the last years, to our knowledge, the spatio-temporal degrees of freedom of a scattering medium have never been used to *spectrally* engineer the point-spread function (PSF) of an ultrashort pulse.

Here, we exploit the MSTM in conjunction with a single SLM to perform arbitrary spatio-spectral PSF engineering. It consists of *(i)* measuring the MSTM to characterize light scattering induced by the medium and *(ii)* numerically filtering a virtual pupil function with a spectrally-dependent mask prior to *(iii)* focusing. Importantly, nearly any arbitrary mask (phase and/or amplitude) can be applied onto the pupil function. This versatility is experimentally shown through the generation of two different spatio-spectral PSFs that both aim at decoupling axial confinement from lateral extent, with multiphoton microscopy applications envisioned. First, we revisit traditional temporal focusing (TF) and show that our approach is not restricted to disperse the pulse along only one spatial dimension as offered by diffraction gratings. Secondly, we report on another TF-like PSF that benefits from the high transverse resolution of a bessel beam but with a better axial confinement. Corresponding spatio-temporal profiles are characterized with a 2-photon fluorescence process.

2. Principle and methods

Focusing light spatially implies that all incident contributions, or k-vectors, arrive at the focal point with the same phase. Stated differently, the Fourier transform of the field in the focal plane – henceforth referred to as the pupil function – has a flat phase. Any modification of this pupil function (in phase and/or amplitude) impacts on the PSF of the optical system. Generally, the pupil function is directly engineered with amplitude and phase masks (with an SLM) placed in the Fourier plane of a first grating where the spectral components of the pulse are spatially separated. Then, a second lens and grating recombine all the wavelengths into a single output beam with a shaped spatio-spectral PSF. However, in presence of multiple scattering, the spatio-spectral coupling is very complex as not simply induced by the grating hence standard pulse shapers are rendered ineffective.

2.1. Experimental setup

A schematic representation of the experimental optical system is shown in Fig. 1. It enables the measurement of the MSTM, generation of the multi-spectral PSF and characterization of in three

Optics EXPRESS

dimensions. A Ti:Sapphire laser source (MaiTai, Spectra Physics, 120 fs pulselength, 800 nm center wavelength, 12.7 nm spectral bandwidth) is used either as a tunable monochromatic source, for characterization, or as a pulsed source with its full bandwidth. Here, the MSTM is measured by sweeping the wavelength as in Ref. [24], but can also be performed using hyper-spectral imaging [28]. The beam is split into two distinct paths: a reference path and a probe path. In the probe path, a phase-only SLM (512×512 pixels, Meadowlark) subdivided in 64×64 macropixels is conjugated with the back focal plane of a microscope objective (Olympus Plan N, 20×, NA 0.40), which illuminates a scattering medium made of ZnO nanoparticles. Sample fabrication consists of diluting the ZnO powder in water and drying it on a coverslip glass (170 μm thick). We prepared a set of samples by changing the volume of the deposited solution, resulting in different thicknesses, all around $\sim$ 100 μm. The transmitted speckle is collected with another microscope objective (Zeiss EC Plan-Neofluar, 40×, NA 1.3). The probe beam leaving the medium is recombined with the reference on a beam splitter (BS) and the hologram is recorded on a CCD camera (CAM1, Allied Vision, Manta G-046). The MSTM elements are obtained by phase-step interferometry of the probe with the reference arm. As the reference and signal arms do not share a common path, phase drifts and fluctuations between them due to temperature gradients and airflow have to be considered. To account for this, the phase drift was monitored and corrected for as shown previously [29].

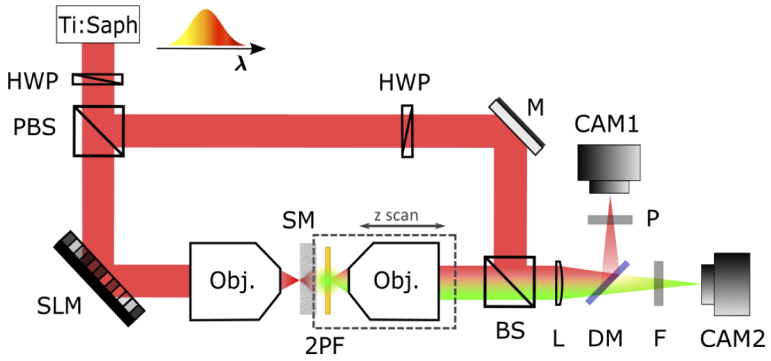

Fig. 1. Experimental setup scheme. HWP: half wave plate, PBS: polarized beam splitter, SLM: spatial light modulator, Obj.: microscope objective, SM: scattering medium, 2PF: 2-photon fluorescence, BS: beam splitter, M: mirror, L: lens, DM: dichroic mirror, F: filter, P: polarizer.

Once measured, the MSTM was stable for few a hours after acquisition. This matrix, in conjunction with the SLM, enabled us to focus light both spatially and spectrally. The corresponding spatio-spectral PSF was characterized by looking at the scattered pulse on CAM1 as in Fig. 2. To infer on the temporal properties of the PSF (Figs. 4 and 5), we used a 2-photon fluorescence process. For this purpose, a solution made of fluorescein is sandwiched between two microscope coverslips (170 μm thick) and placed right behind the scattering medium. The thickness of the fluorescent layer is approximately 10 μm. The fluorescent sample, together with the collection objective, are mounted on a translation stage in order to characterize the beam profile along the z-axis. The 2-photon fluorescence is recorded with an EMCCD camera (CAM2, Andor iXon 3), placed after a dichroic mirror to separate the probe beam from the 2-photon fluorescence, together with additional filters to remove the strong SHG signal emitted by the ZnO medium (longpass, FELH0450, Thorlabs) and to block the probe beam (shortpass, 2× FESH0650, Thorlabs). Note that during the experimental characterization of these 2-photon PSFs the reference arm is blocked.

Optics EXPRESS

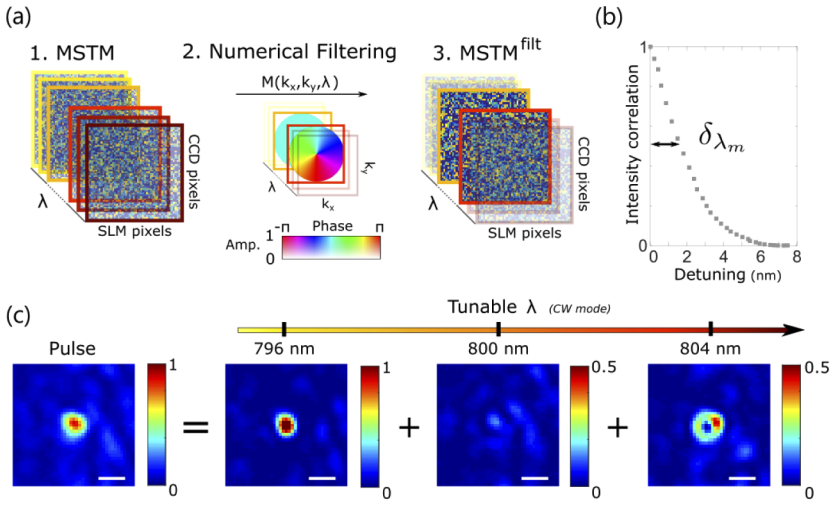

Fig. 2. Principles of spectrally-dependent PSF engineering. (a) Fourier filtering of MSTM with a spectrally-dependent mask $M(k_x, k_y, \lambda)$ gives rise to a new operator, denoted MSTM$^{\text{filt}}$, which can be used as standard MSTMs. (b) Spectral correlation bandwidth of the scattering medium. The latter is experimentally measured by correlating images acquired while scanning the wavelength of the laser in continuous wave mode by steps of 0.3 nm. Half width at half maximum of this curve ($\delta\lambda_m$) defines the spectral correlation bandwidth of the medium. For this medium we found $\delta\lambda_m \simeq 1.6$ nm. (c) Experimental focusing at two wavelengths with two different and arbitrary chosen PSFs. Scale bars 20 μm.

2.2. *Proof-of-concept experiment*

To engineer the multi-spectral PSF of transmitted light, we build a new operator from the experimentally measured MSTM by numerically filtering the pupil (see Fig. 2(a)), as previously shown with monochromatic light [30]. Briefly, we compute the spatial Fourier transform of the experimentally measured output fields, for all the N_{SLM} input modes and N_λ spectral components. Then the pupil is engineered with a spectrally dependent mask $M(k_x, k_y, \lambda)$, allowing for multi-spectral PSF engineering through thick scattering media. We must specify here that both phase and/or amplitude of the mask are tunable. Finally, an inverse Fourier transform of the filtered pupil function is performed to return to real space. The latter corresponds physically to the focal plane where the MSTM was measured. This last operation generates a filtered multi-spectral TM, denoted in the following MSTM$^{\text{filt}}$. A more detailed description of the procedure is provided in Appendix A in Supplement 1.

In Fig. 2 we demonstrate the MSTM$^{\text{filt}}$ capability through a proof-of-concept experiment. The scattering medium used here provides $N_\lambda = 8$ spectral degrees of freedom, and thus a set of 8 monochromatic TMs are measured to describe the pulse propagation through the medium. For the sake of demonstration, we filtered only two TMs over the N_λ available, respectively with, a flat ($\lambda = 796$ nm) and a spiral ($\lambda = 804$ nm) phase mask.Phase conjugation of the two TMs at $\lambda = 796$ nm and $\lambda = 804$ nm enables arbitrary spatial focusing of the two wavelengths on either the same spatial position or on two separate positions. Here the two wavelengths are spatially focused on the same position. As detailed in [26] the two input fields calculated from phase conjugation are algebraically summed and the resulting phase is displayed onto the SLM. As shown in Fig. 2(c), such shaping focuses the transmitted pulse on the camera. A scan in wavelength exhibits a diffraction-limited focus at $\lambda = 796$ nm and a donut-like shape at $\lambda = 804$ nm in agreement with the masks applied in k-spaces of the corresponding matrices. The experimentally obtained focused spots may look distorted because part of the light is not

Optics EXPRESS

controlled and create a background speckle [30]. For the other spectral components, no specific focus is obtained: at these corresponding wavelengths the SLM hologram generates a speckle pattern. As an example, we report the output intensity at $\lambda = 800$ nm. Similar results were also obtained using a metasurface but it offers a much lower spectral resolution [31]. One advantage of our approach is its high degree of reconfigurability; with the same medium and by simply changing the incident wavefront with an SLM, a new spatio-spectral PSF can be generated.

3. Experimental results

3.1. Motivations

In microscopy, a widespread application of pulse shaping is simultaneous spatial and temporal focusing (TF) [11,32]. It consists of shaping the beam in such a way that its pulse duration varies along the propagation direction, and that the shortest duration occurs only close to the focal plane of the illumination objective [Fig. 3(a)]. It improves significantly the axial sectioning of the 2-photon fluorescence excitation, with various applications in neuroscience [33,34], since the 2-photon signal is inversely proportional to the pulse duration. The key optical part in temporal focusing is its dispersive element which generates the spatio-spectral coupling. Generally, a diffraction grating is used as dispersive element [5] but alternatives based on digital micromirror devices have also been proposed [35]. In both cases, the spatial dispersion is done along a single axis spanning a line as represented in Fig. 3.a or, with an objective lens focusing all spectral components at its focal plane, where all wavelengths overlap and the shortest pulse length is reached. As such, the technique only applies in free space where the spatio-spectral coupling induced by the grating is known.

In our method, presented in Fig. 3(b), the diffraction grating is replaced by a thick scattering medium which naturally provides the spatio-spectral coupling. Its control is then achieved with a SLM and knowledge of the MSTM. Once the matrix is measured, the pupil function is numerically filtered with a spectrally-dependent mask $M(k_x, k_y, \lambda)$. The mask is obtained by dividing the pupil (corresponding to the entire accessible k-space) into N_λ sub-pupils, each defining also a spectral component of the pulse. For instance, the mask M may have an helical shape as represented in Fig. 3(b). Importantly, this scheme provides many ways of engineering the spatial dispersion of the pulse, in contrast with a diffraction grating that gives a unidirectional mapping either spanning a line [11,32] or filling the full k-space [36]. This translates here into a more isotropic PSF along the z-axis as reported on Fig. 3(e).

To show the versatility of MSTM^{filt} we report on the experimental realization of two different temporally focused beams which both aim at decoupling axial from lateral resolution. In a first example, we implement the MSTM-TF introduced in Fig. 3(b) that improves the axial confinement. In a second example, we reduce the axial extension of a Bessel-like beam with a different pupil mask. In both cases, we infer the temporal and spatial properties of the generated PSFs by characterizing with a 2-photon excited fluorescence process (Figs. 4 and 5).

3.2. MSTM^{filt}-based axial temporal focusing

As a first experimental demonstration, we generate TF using thick scattering media. As explained in Fig. 3(b), our approach consists of filling the pupil, or entire k-space, with N_λ sub-pupils. The idea is to spectrally combine the spatial properties of two PSFs, coined High NA and Low NA, into a third one, MSTM-TF, which aims at achieving temporal focusing. More specifically, these three PSFs are obtained from the following pupil functions:

- High NA, the pupil mask fills the whole aperture []see top panel Fig. 4(a)]. This mask is applied on all the TMs, regardless their wavelength. This mask produces a beam with waist w_0 and Rayleigh length z_R. The two are related through the numerical aperture

Optics EXPRESS

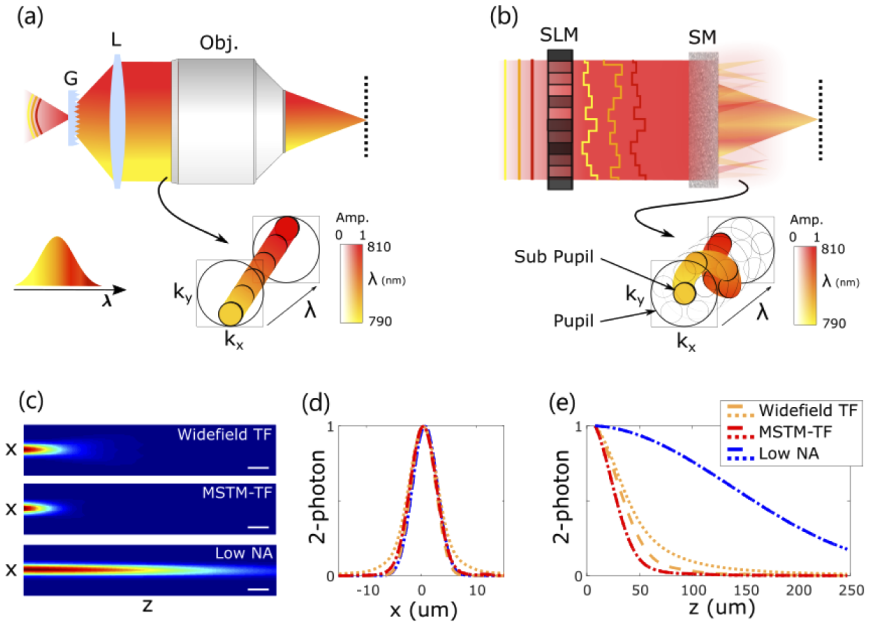

Fig. 3. Temporally focused (TF) light-shaping techniques. (a) Widefield TF. (Top panel) Schematic view of widefield TF using a grating and an objective lens. (Bottom panel) The pulse spectrum and its spatial unidirectional spreading in the pupil plane (corresponding physically to the back focal plane of the objective). (b) MSTM-TF. (Top panel) Scheme of our MSTM approach based on a scattering medium and an SLM. Each spectral component of the pulse is independently controlled with an SLM. (Bottom panel) The mask applied in a virtual pupil (accessible by computing a Fourier transform). (c) Comparison of expected PSFs in free space. Numerical simulations are obtained by Fourier transforming the mask "Widefield-TF", "MSTM-TF" and "Low NA" – for all the spectral components of the pulse and summing them incoherently. We propagate the field and retrieve the longitudinal beam profile using diffraction theory (Fresnel approximation). While the (d) lateral profile of the "Widefield TF" and the MSTM-TF is similar to the Low NA, the (e) axial confinement is significantly improved using TF. Regarding planes yz (dasked lines) and xz (dotted lines), MSTM-TF has a more isotropic PSF than the Widefield-TF approach. G: grating, L: lens, Obj.: microscope objective, SLM: spatial light modulator, SM: scattering medium. Scale bars 2 μm.

Optics EXPRESS

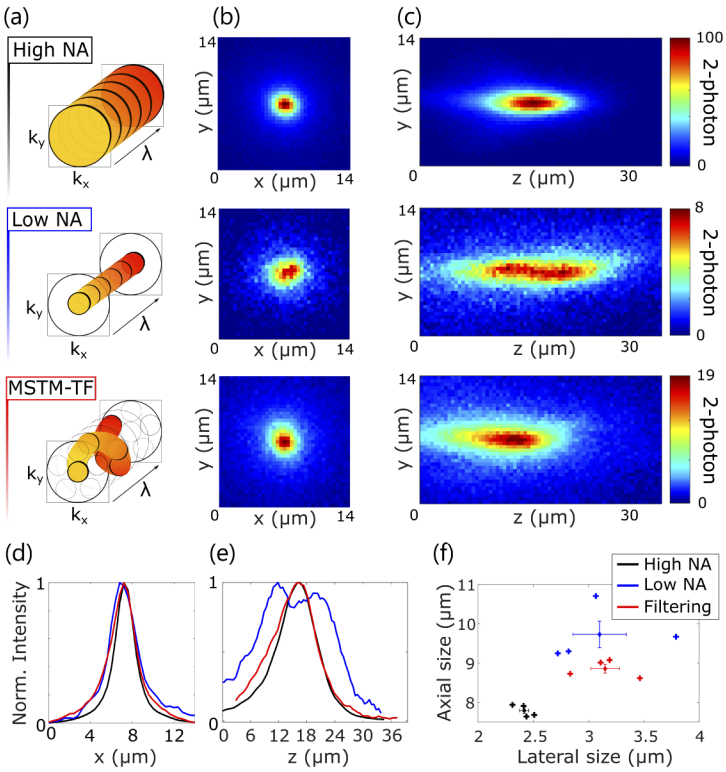

Fig. 4. Experimental demonstration of temporally focused light generation with a thick scattering medium (MSTM-TF). It combines two PSFs, termed High NA and Low NA (a) Spectrally dependent masks computed onto the virtual pupil accessible from the Fourier transform of the output field, captured in the MSTM. (b) Lateral profiles of the corresponding generated PSFs (projection of the beam onto z-axis). (c) Axial profiles (projection of the beam onto y-axis). (d) Lateral profiles (projection of (b) onto y-axis). (e) Axial profiles (projection of (c) onto x-axis). (f) Lateral and axial sizes of each PSF for 4 different spatial positions. The "lateral size" is $\sqrt{\sigma_{2_x}^2 + \sigma_{2_y}^2}$, where σ_{2_x} and σ_{2_y} are the standard deviations of the transverse intensity distribution of the beam along the x- and y-axis respectively. We also report the mean and standard deviation values for each case.

Optics EXPRESS

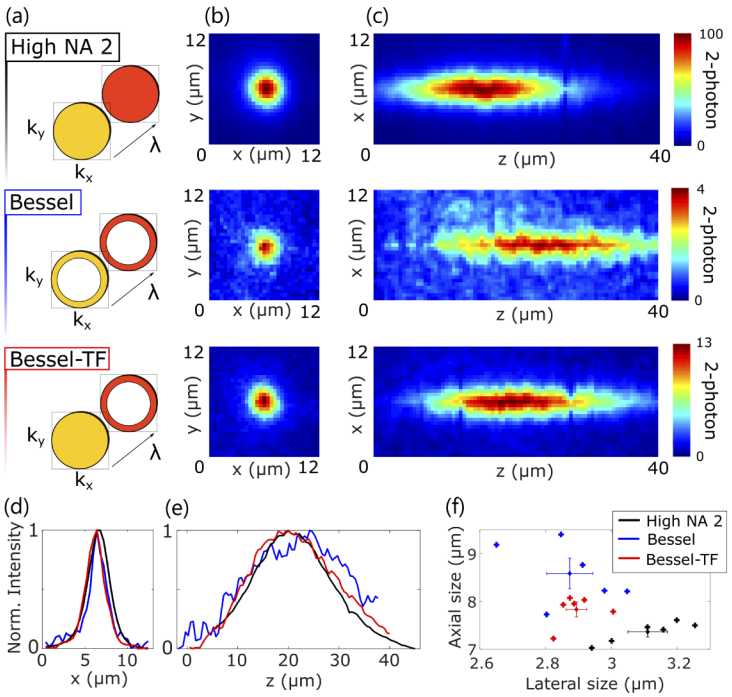

Fig. 5. Another example of temporally focused beam with a scattering medium (Bessel-TF). It combines two PSFs, denoted High NA and Bessel – Experimental Results – (a) Spectrally dependent masks computed onto the virtual pupil accessible from the Fourier transform of the output field, captured in the MSTM. The annulus ring has an inner radius = $0.67k_1$, where k_1 is the outer radius (i.e. size of the aperture). (b) Lateral profiles of the corresponding generated PSFs (projection of the beam onto z-axis). (c) Axial profiles (projection of the beam onto y-axis). (d) Lateral profiles (projection of (b) onto y-axis). (e) Axial profiles (projection of (b) onto x-axis). (f) Lateral and axial sizes of each PSF for 6 different output spatial positions. We also report the mean and standard deviation values for each case.

NA $\propto w_0/z_R$. In Fig. 4(a), the numerical aperture is around NA $\simeq$ 0.6 (see further information in Appendix B in Supplement 1).

- Low NA, the same filtering is done with sub-pupil, three times smaller than the pupil [see middle panel Fig. 4(a)]. Compared to the previous situation this mask produces a beam with larger waist and Rayleigh length. This pupil corresponds to a numerical aperture of NA $\simeq$ 0.3.

- MSTM-TF, sub-pupils (same sizes as Low NA ones) are centered at a different position for different wavelengths, inside the pupil. Sub-pupils are positioned in such a way that they cover the pupil [see bottom panel Fig. 4(a)]. This mask produces a beam with a waist comparable to Low NA but a reduced Rayleigh length.

The three cases are experimentally compared in Fig. 4. The scattering medium is characterized by $\delta\lambda_m \simeq 1.8$ nm. Consequently, for our probe spectrum we have $N_\lambda = 6$, hence a set of 6 monochromatic TMs were measured to control the full propagation of the pulse spectrum through the medium. Quantitatively, we estimate lateral and axial sizes with the standard deviations of the corresponding distributions. With the same MSTM we repeat the procedure and focus light on three other output spatial positions. Results are plotted in Fig. 4(f) demonstrating the

Optics EXPRESS

interest of using such pupil mask function: whereas the lateral size of the MSTM-TF filtering is very similar to Low NA, its axial confinement is improved. The 2-photon signal through thick scattering media is very weak, leading to long exposure time and limiting the number of positions one can measure within the medium stability time. The full three-dimensional characterization of a single PSF [which corresponds to a single point in the graph in Fig. 4(f)] took approximately ~ 40 min. We report in Appendix C in the Supplement 1 a statistical analysis of the experimental data plotted in Fig. 4(f).

3.3. *MSTM^{filt}-based lateral temporal focusing*

Since the generation of these PSFs requires only two independent spectral components, we opted for a thinner medium than the one used in the previous experiment, with a $\delta\lambda_m \simeq 7$ nm, corresponding to $N_\lambda = 2$, and controlled with a set of 2 monochromatic TMs. For the PSF Bessel-TF, the two wavelengths are not equally filtered in terms of energy: only the highest spatial frequencies are used at one λ whereas the full pupil is taken at the other one. To compensate for this, we weighted the sum of the two input fields at each wavelength to ensure equal intensity at the focus, which is an additional degree of control allowed by our technique. Since the medium is thinner, more light is transmitted, which allows speeding up the acquisition.

In a second experiment using a different scattering medium, we combine two other PSFs coined High NA2 and Bessel, and present another example, Bessel-TF, for decoupling the lateral from axial profiles of the beam. These three PSFs are obtained from the following pupil functions:

- High NA2, a large pupil mask is used to filter all the TMs [see top panel Fig. 5(a)]. Note that the size of the pupil is smaller than the High NA filtering performed in Fig. 4. This pupil's size corresponds to a numerical aperture of NA $\simeq$ 0.5.
- Bessel, the mask corresponds to an annulus with controllable inner and outer radius [see middle panel Fig. 5(a)]. This mask generates a Bessel-like beam whose central lobe is narrower than High NA beam. But this is at the cost of the axial confinement.
- Bessel-TF, one TM is filtered with a High NA mask and the other one with a Bessel mask [see bottom panel Fig. 5(a)]. Such pupil creates a tight focus spot with improved confinement compared to the Bessel case.

The three cases are experimentally compared in Fig. 5. Their lateral and longitudinal extensions are retrieved with the same method as before. As one can notice, the Bessel PSF (middle panel) is very noisy. The associated numerical filtering only retains the high spatial frequencies: all k>0.67k_1, where k_1 is the radius of the pupil. Most of the light (at low spatial frequencies) is rejected and the resulting PSF has a very low signal-to-background ratio (this has been further studied in the Supplement 1 [30]). In theory, such PSF is diffraction free, meaning that the longitudinal extent is very large. We report in Appendix D i the Supplement 1 complementary simulations and analysis of these PSFs. Due to the background speckle, this expected property is really depreciated. Another downside is that we cannot accurately estimate its lateral and axial sizes [blue crosses in Fig. 5(f)]. However, while a somewhat weaker effect is found for this second example of temporally-focused light shaping, it appears that the spectral combination of High NA2 and Bessel PSFs provides independent controllable lateral and longitudinal properties. This is further demonstrated in Appendix C in the Supplement 1 with a statistical analysis of the experimental data.

4. Discussion and conclusion

Several conditions should be met to successfully and efficiently engineer spatio-temporal PSFs through scattering media. A first important point to consider is the spatio-spectral coupling

Optics EXPRESS

induced by the scattering material. Our ability to tune the propagation of the beam strongly relies on the number of degrees of freedom, both spatial and spectral, in the system. On the one hand, the number of controlled spatial modes with the SLM translates directly into the quality of the generated beam in the spatial domain. Here we measured the MSTM for a basis of $N_{SLM} = 4096$ orthogonal modes (Hadamard basis), which corresponds to an acquisition time of ~ 2 min for a single TM at a given λ. To retrieve the full MSTM, this operation must be repeated N_λ times. This is not a major issue here since the medium proved to be stable for few hours. Note that the measurement can be sped up considerably using hyperspectral techniques [28] or swept-wavelength interferometry [37]. On the other hand, the spectral bandwidth of the medium (and consequently the number of spectral channels N_λ) is a property of the scattering medium itself. N_λ scales as $\propto (\Delta\lambda^{\text{laser}} L^2)/(\lambda^2 l_t)$ and can be adjusted with the thickness of the medium L or the transport mean free path l_t [38,39]. However, these quantities also affect the total transmission of the light $T \propto l_t/L$ in the diffusive regime. In Figs. 4 and 5, we characterized the spatio-spectral PSFs by measuring the 2-photon fluorescence signal, which scales as the square of the excitation intensity. Simply put, doubling the thickness of the medium increases N_λ by a factor 4 but on the other hand the total 2-photon signal is 4 times lower. Therefore in thick scattering media, such as our layers of white paint, there is a trade-off between the transmitted intensity and the number of independent spectral components one can control, which limits the technique to the generation of relatively simple spectral PSFs. However, our approach is very general and may apply to other complex media, such as multimode fibers (MMFs). In a MMF, interference among the guided modes creates wavelength-dependent speckle patterns upon illumination with a coherent source. The spectral correlation width of the speckle $\delta(\lambda)$ scales inversely with the length of the fiber for a fixed numerical aperture [40,41], with almost no penalty on the transmitted intensity. Since optical fibers have been optimized for long distance transmission with minimal loss, long fibers can be used to provide very small $\delta(\lambda)$ without altering the total transmission. Such property has already been extensively exploited for turning fibers into high resolution spectrometer [42,43] but may be amenable to spatio-spectral pulse shaping with similar spectral resolution.

In conclusion, we have reported on the formulation of an operator, built upon the experimentally measured MSTM, that enables deterministic spatio-spectral focusing of any arbitrary PSF after propagation through a multiple scattering sample. The spectral resolution is given by the dispersion of the medium and the focusing efficiency by the number of controlled pixels on a single input SLM. We have illustrated the strength of this technique by characterizing their transverse and longitudinal properties in a temporal focusing application. The method we propose can readily be extended to other complex media, in particular to multimode fibers that have much higher transmission with similar spectral properties. The possibility of arbitrarily generating complex multi-spectral PSF through multiply scattering media opens up new opportunities in several fields, in particular for microscopy as well as coherent control and nanophotonics.

Funding. European Research Council (Grant SMARTIES - 724473); Agence Nationale de la Recherche (ANR-10-IDEX-0001-02 PSL*, ANR-10-LABX-0010); Australian Research Council (DE210100934).

Acknowledgment. SG is a member of the Institut Universitaire de France. HBdA was supported by the LabEx ENS-ICFP: ANR-10-LABX-0010/ANR-10-IDEX-0001-02 PSL*.

Disclosures. The authors declare no conflicts of interest.

Data availability. Data underlying the results presented in this paper are not publicly available at this time but may be obtained from the authors upon reasonable request.

Supplemental document. See Supplement 1 for supporting content.

References

1. A. M. Weiner, "Femtosecond pulse shaping using spatial light modulators," Rev. Sci. Instrum. **71**(5), 1929–1960 (2000).
2. A. Weiner, D. Leaird, G. P. Wiederrecht, and K. A. Nelson, "Femtosecond pulse sequences used for optical manipulation of molecular motion," Science **247**(4948), 1317–1319 (1990).

Optics EXPRESS

3. G. Baxter, S. Frisken, D. Abakoumov, H. Zhou, I. Clarke, A. Bartos, and S. Poole, "Highly programmable wavelength selective switch based on liquid crystal on silicon switching elements," in *2006 Optical Fiber Communication Conference and the National Fiber Optic Engineers Conference*, (IEEE, 2006), p. 3.
4. Y. Silberberg, "Quantum coherent control for nonlinear spectroscopy and microscopy," Annu. Rev. Phys. Chem. **60**(1), 277–292 (2009).
5. E. Papagiakoumou, E. Ronzitti, and V. Emiliani, "Scanless two-photon excitation with temporal focusing," Nat. Methods **17**(6), 571–581 (2020).
6. B. Sun, P. S. Salter, C. Roider, A. Jesacher, J. Strauss, J. Heberle, M. Schmidt, and M. J. Booth, "Four-dimensional light shaping: manipulating ultrafast spatiotemporal foci in space and time," Light: Sci. Appl. **7**(1), 17117 (2018).
7. H. Vincenti and F. Quéré, "Attosecond lighthouses: How to use spatiotemporally coupled light fields to generate isolated attosecond pulses," Phys. Rev. Lett. **108**(11), 113904 (2012).
8. G. Pariente and F. Quéré, "Spatio-temporal light springs: extended encoding of orbital angular momentum in ultrashort pulses," Opt. Lett. **40**(9), 2037–2040 (2015).
9. A. Sainte-Marie, O. Gobert, and F. Quere, "Controlling the velocity of ultrashort light pulses in vacuum through spatio-temporal couplings," Optica **4**(10), 1298–1304 (2017).
10. J. P. Palastro, J. L. Shaw, P. Franke, D. Ramsey, T. T. Simpson, and D. H. Froula, "Dephasingless laser wakefield acceleration," Phys. Rev. Lett. **124**(13), 134802 (2020).
11. G. Zhu, J. van Howe, M. Durst, W. Zipfel, and C. Xu, "Simultaneous spatial and temporal focusing of femtosecond pulses," Opt. Express **13**(6), 2153–2159 (2005).
12. D. Oron and Y. Silberberg, "Spatiotemporal coherent control using shaped, temporally focused pulses," Opt. Express **13**(24), 9903–9908 (2005).
13. T. Feurer, J. C. Vaughan, R. M. Koehl, and K. A. Nelson, "Multidimensional control of femtosecond pulses by use of a programmable liquid-crystal matrix," Opt. Lett. **27**(8), 652–654 (2002).
14. J. C. Vaughan, T. Feurer, and K. A. Nelson, "Automated two-dimensional femtosecond pulse shaping," J. Opt. Soc. Am. B **19**(10), 2489–2495 (2002).
15. T. Feurer, J. C. Vaughan, and K. A. Nelson, "Spatiotemporal coherent control of lattice vibrational waves," Science **299**(5605), 374–377 (2003).
16. R. Piestun and D. A. Miller, "Spatiotemporal control of ultrashort optical pulses by refractive–diffractive–dispersive structured optical elements," Opt. Lett. **26**(17), 1373–1375 (2001).
17. D. H. Froula, D. Turnbull, A. S. Davies, T. J. Kessler, D. Haberberger, J. P. Palastro, S.-W. Bahk, I. A. Begishev, R. Boni, S. Bucht, and J. Katz, "Spatiotemporal control of laser intensity," Nat. Photonics **12**(5), 262–265 (2018).
18. J. W. Goodman, *Speckle phenomena in optics: theory and applications* (Roberts and Company Publishers, 2007).
19. J. Aulbach, B. Gjonaj, P. M. Johnson, A. P. Mosk, and A. Lagendijk, "Control of light transmission through opaque scattering media in space and time," Phys. Rev. Lett. **106**(10), 103901 (2011).
20. O. Katz, E. Small, Y. Bromberg, and Y. Silberberg, "Focusing and compression of ultrashort pulses through scattering media," Nat. Photonics **5**(6), 372–377 (2011).
21. E. E. Morales-Delgado, S. Farahi, I. N. Papadopoulos, D. Psaltis, and C. Moser, "Delivery of focused short pulses through a multimode fiber," Opt. Express **23**(7), 9109–9120 (2015).
22. D. J. McCabe, A. Tajalli, D. R. Austin, P. Bondareff, I. A. Walmsley, S. Gigan, and B. Chatel, "Spatio-temporal focusing of an ultrafast pulse through a multiply scattering medium," Nat. Commun. **2**(1), 447–455 (2011).
23. M. Mounaix, H. Defienne, and S. Gigan, "Deterministic light focusing in space and time through multiple scattering media with a time-resolved transmission matrix approach," Phys. Rev. A **94**(4), 041802 (2016).
24. D. Andreoli, G. Volpe, S. Popoff, O. Katz, S. Grésillon, and S. Gigan, "Deterministic control of broadband light through a multiply scattering medium via the multispectral transmission matrix," Sci. Rep. **5**(1), 10347 (2015).
25. S. Popoff, G. Lerosey, R. Carminati, M. Fink, A. Boccara, and S. Gigan, "Measuring the transmission matrix in optics: an approach to the study and control of light propagation in disordered media," Phys. Rev. Lett. **104**(10), 100601 (2010).
26. M. Mounaix, D. Andreoli, H. Defienne, G. Volpe, O. Katz, S. Grésillon, and S. Gigan, "Spatiotemporal coherent control of light through a multiple scattering medium with the multispectral transmission matrix," Phys. Rev. Lett. **116**(25), 253901 (2016).
27. M. Mounaix, D. M. Ta, and S. Gigan, "Transmission matrix approaches for nonlinear fluorescence excitation through multiple scattering media," Opt. Lett. **43**(12), 2831–2834 (2018).
28. A. Boniface, I. Gusachenko, K. Dholakia, and S. Gigan, "Rapid broadband characterization of scattering medium using hyperspectral imaging," Optica **6**(3), 274–279 (2019).
29. M. Plöschner, B. Straka, K. Dholakia, and T. Čižmár, "Gpu accelerated toolbox for real-time beam-shaping in multimode fibres," Opt. Express **22**(3), 2933–2947 (2014).
30. A. Boniface, M. Mounaix, B. Blochet, R. Piestun, and S. Gigan, "Transmission-matrix-based point-spread-function engineering through a complex medium," Optica **4**(1), 54–59 (2017).
31. Z. Zhao, M. Pu, H. Gao, J. Jin, X. Li, X. Ma, Y. Wang, P. Gao, and X. Luo, "Multispectral optical metasurfaces enabled by achromatic phase transition," Sci. Rep. **5**(1), 15781 (2015).
32. E. Tal, D. Oron, and Y. Silberberg, "Improved depth resolution in video-rate line-scanning multiphoton microscopy using temporal focusing," Opt. Lett. **30**(13), 1686–1688 (2005).

Optics EXPRESS

33. E. Papagiakoumou, V. De Sars, D. Oron, and V. Emiliani, "Patterned two-photon illumination by spatiotemporal shaping of ultrashort pulses," Opt. Express **16**(26), 22039–22047 (2008).
34. T. Schrödel, R. Prevedel, K. Aumayr, M. Zimmer, and A. Vaziri, "Brain-wide 3d imaging of neuronal activity in caenorhabditis elegans with sculpted light," Nat. Methods **10**(10), 1013–1020 (2013).
35. Y. Da Sie, C.-Y. Chang, C.-Y. Lin, N.-S. Chang, P. J. Campagnola, and S.-J. Chen, "Fast and improved bioimaging via temporal focusing multiphoton excitation microscopy with binary digital-micromirror-device holography," J. Biomed. Opt. **23**(11), 1–8 (2018).
36. A. Vaziri and C. V. Shank, "Ultrafast widefield optical sectioning microscopy by multifocal temporal focusing," Opt. Express **18**(19), 19645–19655 (2010).
37. M. Mounaix and J. Carpenter, "Control of the temporal and polarization response of a multimode fiber," Nat. Commun. **10**(1), 5085–5088 (2019).
38. B. Shapiro, "Large intensity fluctuations for wave propagation in random media," Phys. Rev. Lett. **57**(17), 2168–2171 (1986).
39. J. Aulbach, "Spatiotemporal control of light in turbid media," Ph.D. thesis, University of Twente (2013).
40. E. G. Rawson, J. W. Goodman, and R. E. Norton, "Frequency dependence of modal noise in multimode optical fibers," J. Opt. Soc. Am. **70**(8), 968–976 (1980).
41. W. Freude, C. Fritzsche, G. Grau, and L. Shan-da, "Speckle interferometry for spectral analysis of laser sources and multimode optical waveguides," J. Lightwave Technol. **4**(1), 64–72 (1986).
42. B. Redding and H. Cao, "Using a multimode fiber as a high-resolution, low-loss spectrometer," Opt. Lett. **37**(16), 3384–3386 (2012).
43. B. Redding, M. Alam, M. Seifert, and H. Cao, "High-resolution and broadband all-fiber spectrometers," Optica **1**(3), 175–180 (2014).